JOURNAL OF APPLIED ELECTROCHEMISTRY 4 (1974) 259–262

Analysis of porous alkaline Cd-electrodes. II. Potential recovery transients after a period of discharge

PER SELÅNGER

Division of Chemical Technology, The Lund Institute of Technology, Chemical Centre, Lund, Sweden

Received 1 January 1974

The recovery of the diffusion potential after a period of discharge is analysed for porous Cd-electrodes. A composite process with discharge–idle time and discharge is simulated and compared with an experimental process. The general influence of porosity on charge capacity is examined in a charge porosity diagram.

Nomenclature

Symbols

- a electrolyte activity
- c concentration of the binary electrolyte KOH mol cm^{-3}
- D diffusion coefficient, $cm^2\ s^{-1}$
- F the Faraday constant, 96487 As per mol equiv.
- l electrode thickness, cm
- R universal gas constant, 8·3143 $J\ K^{-1}\ mol^{-1}$
- t time, s
- T temperature, K
- x position co-ordinate, inside the electrode, cm

Greek

- γ activity coefficient
- η overpotential

Subscripts

- b bulk electrolyte
- d diffusion
- eff effective
- o initial time
- w water as solvent

1. Introduction

Until now there has been no analysis of porous electrodes in the current free state after an active current period. The recovery of the electrodes after an active current state is of great importance in various engine-cranking applications. Therefore it is of interest to analyse the currentless state in order to be able to simulate a chain of cranking and idle-time periods. A specification of general cranking conditions for various engines is presented by U. Falk and A. Salkind [1]. In this work some results are shown for the porous electrodes which are described earlier in an analysis of transients in the active state. [2]

In this work the diffusion of reactants from the bulk electrolyte into the electrodes is the considered potential recovery mechanism. The electrodes are also considered to be free from porosity changes during the recovery time. Diffusion is supposed to be of importance at intervals of a half second to about an hour. The technical cranking procedures are mostly within the specified interval of time. Here the potential transients are conclusively interpreted as pure concentration potential transients.

2. The model

The basic model is the same as described in an earlier paper [2]. As there is no species source in a currentless state the mass conservation equation for a one-dimensional electrode, with a binary electrolyte, will be as follows:

$$\frac{\partial c}{\partial t} = D_{\text{eff}}\left(1 - \frac{\mathrm{d}\ln c_{\text{w}}}{\mathrm{d}\ln c}\right)\frac{\mathrm{d}^2 c}{\mathrm{d}x^2} \qquad (1)$$

The concentration transients inside the electrodes are obtained from the solution of Equation 1 for the following boundary conditions, at the time t_0,

$$c(x, t_0) = c_0(x) \qquad 0 \leqslant x \leqslant 1 \qquad (2)$$

which is the concentration profile inside the electrode at the current breaking moment t_0.

At the collector $x = 1$ the insulation condition (Equation 3) is valid,

$$\frac{\mathrm{d}c(l,t)}{\mathrm{d}x} = 0 \qquad t \geqslant t_0 \qquad (3)$$

The bulkside condition $x = 0$ is for a well-stirred bulk electrolyte,

$$c(0, t) = c_{\text{b}} \qquad t \geqslant t_0 \qquad (4)$$

Analytical solutions to this problem are in general not easy to obtain, because of the general and non-linear form of the initial distribution condition (Equation 2).

The diffusion potential transient is obtained from the numerically solved concentration profiles calculated with the Nernst equation (Equation 5)

$$\eta_{\text{d}} = \frac{RT}{nF}\ln\frac{a_1}{a_2} \qquad (5)$$

where a_1 is the electrolyte activity at the reference electrode position and a_2 is the minimum activity inside the electrode. The latter activity is calculated from the concentration profile according to Equation 6. The minimum concentration is not in general equivalent to the minimum activity [5].

$$a = \gamma c \qquad (6)$$

The solution to Equation 1 with the given boundary conditions is solved by the numerical method mentioned earlier [2].

3. Results and discussion

Fig. 1 shows experimental and simulated potential recovery transients for some electrodes.

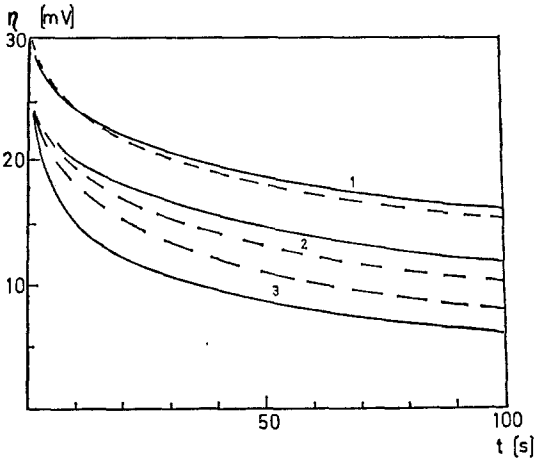

Fig. 1. Experimental and simulated diffusion potential recovery transients after deep discharges for three different porous Cd-electrodes. Curve 1 is an electrode with the thickness $l = 0{\cdot}080$ cm and the porosity $\varepsilon = 0{\cdot}35$, curve 2 an electrode with $l = 0{\cdot}1$ cm and $\varepsilon = 0{\cdot}65$. Curve 3 and electrode with $l = 0{\cdot}15$ cm and $\varepsilon = 0{\cdot}75$. The given porosities are mean porosities at final discharge. $D_{\text{eff}} = \varepsilon^{3/2}$ D is applied. Simulated curves are shown as dotted lines.

The differences in recovery between the electrodes shown are explained by differences in mass transport properties. The curves 1 to 3 show the influence of porosity on the recovery dynamics. As one would expect, the high porosity electrodes have the best recovery ability. The coefficient used for the calculation of the effective diffusion coefficient, D_{eff}, was $\varepsilon^{3/2}$ [6]. The initial porosity and concentration profiles were calculated with the dynamical model [2] described earlier.

Fig. 2 shows an experimental and simulated chain of discharge–recovery and discharge, in order to demonstrate the potential possibility to describe complex transient processes with the model simulation technique. The simulation of the processes just described for porosities greater than 0·45, was successful. Deviations appeared for the lower porosities in the simulation of the second discharge period. The model predicted, in general, lower polarizations than were measured. The unsuccessful simulation of a low

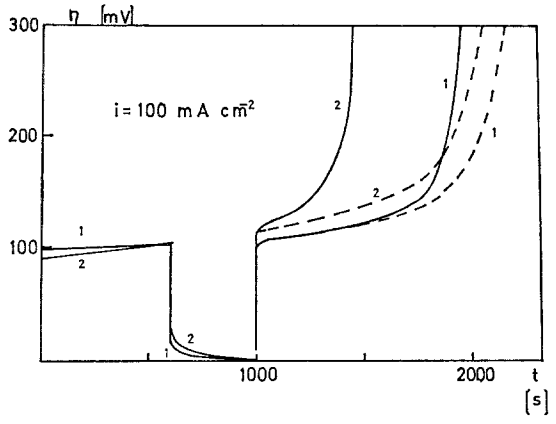

Fig. 2. Comparison of experimental and simulated combined processes composed of a 600 s long discharge, 400 s recovery and a final discharge. Dotted curves are simulations. Curve 1 is an electrode with $\varepsilon = 0{\cdot}53$, $l = 0{\cdot}190$ cm. Curve 2 is a low porosity electrode with $\varepsilon = 0{\cdot}41$ and $l = 0{\cdot}180$ cm.

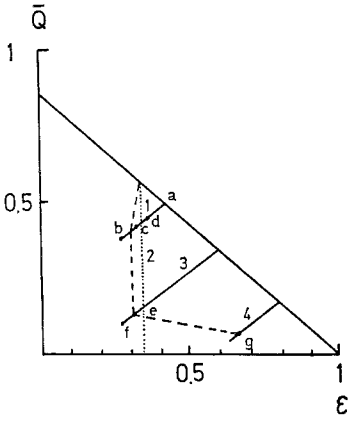

Fig. 3. A charge – porosity diagram for $Cd/Cd(OH)_2$ with Fe_2O_3 as the inert material. The full charge line is drawn for 90 w % CdO and 10% Fe_2O_3. The characteristic discharge slope $d\bar{Q}/d\varepsilon$ is 0·745. The dotted line corresponds to final states at 75 mA cm^{-2} from fully charged states.

porosity electrode is shown in the diagram. A possible explanation for the failure can be that the basic model does not accurately describe the controlling processes, in the region where the pores are no longer properly connected.

A possible interpretation of the unsuccessful simulation could be that the active surface was blocked by precipitated $Cd(OH)_2$ from a supersaturated cadmiate electrolyte during the idle time. The effect of marginal precipitation can be expected to be greatest for low porosity electrodes because of the disconnected pores. This has been discussed previously [2].

A study of the situation in a charge–porosity diagram can give a broader view. The charge–porosity diagram has been described earlier in this journal [3].

The critical porosity is defined as the porosity where an electrode almost loses reaction activity in the fully charged state. The region where the porosity becomes critical is in the region where the electrolyte phase begins to be disconnected by close packing of the solid phase. The characteristic critical porosity for this electrode material and preparations is found to be close to 0·34 This limiting value is shown as the vertical line 2 in Fig. 3, which shows a low porosity electrode on the discharge line 1. The low porosity electrode follows line 1 at discharge from the initial point *a* to the final point *b* in a pure discharge process at 75 mA cm^{-2}. Point *c* is obtained as the final point in a composite process with discharge to *d*, one hour idle at *d* and a final discharge to *c* where the electrode is polarized infinitely.

Line 3 shows an electrode with the initial porosity of 0·60, which is the usual level in commercial electrodes; the corresponding final state is predicted to point *e*. The discharge efficiency for the last process is calculated from the diagram to be about 60%. In practice such electrodes will have around 70% utilization [4]. The latter efficiency is shown as point *f*.

High porosity electrodes, as pointed out earlier do not show the previously discussed effects which can also be expected from the charge–porosity diagram. Line 4 for an electrode with a porosity of 0·75 which nowhere reaches the limiting value $\varepsilon = 0{\cdot}34$ within the obtained efficiency 0·60. The latter corresponds to point *g*. The dotted boundary line *h* shows the final states for the examined electrodes at the constant current level of 75 mA cm^{-2}.

4. Conclusions

The recovery of the potential can be predicted by means of numerical mass transfer models for known initial concentration and porosity profiles inside porous electrodes. It should be

possible to analyse commercial electrode materials in the same way as in this analysis in combination with the previous analysis. The analysis could also be implemented on other similar electrode systems such as alkaline zinc and iron electrodes and on the lead–acid system. The charge–porosity diagram can be regarded as an efficient means of storing comprehensive information on electrode systems.

References

[1] U. Falk and A. Salkind, 'Alkaline Storage Batteries', Wiley (1969) pp. 466–78.
[2] P. Selånger, *J. Appl. Electrochem.*, **4** (1974) 249.
[3] P. Selånger, *J. Appl. Electrochem.*, **4** (1974) 263.
[4] U. Falk and A. Salkind, 'Alkaline Storage Batteries', Wiley (1969) p. 332.
[5] G. C. Åkerlöf and P. Bender, *J. Am. Chem. Soc.*, **70** (1948) 2366.
[6] E. E. Petersen, 'Chemical Reaction Analysis', Prentice Hall (1965) p. 121.